

Adapting multilooking for joint radiometrical and geometrical SAR image enhancement

G. Schwarz¹, D. Espinoza Molina¹, H. Breit¹, M. Datcu^{1,2}

¹German Aerospace Center (DLR), Remote Sensing Technology Institute, 82234 Wessling, Germany

²Paris Institute of Technology GET/Télécom Paris, 75013 Paris, France

Abstract—Many SAR processors deliver separate products serving either the radiometrical or the geometrical demands of the user community. However, when it comes to reliable feature extraction and classification of remote sensing SAR images, we need both good radiometrical and geometrical image quality as a pre-requisite for lasting results. Therefore, we suggest a new common product characterized by high joint radiometrical and geometrical quality. This new product can be generated by adapting the applied multilooking and by careful signal processing. As an example, we demonstrate classification results from high resolution SAR images of the German TerraSAR-X mission.

Index Terms—Down-sampling, image enhancement, multi-look, radiometry, remote sensing, resolution, SAR, speckle, TerraSAR-X.

I. INTRODUCTION

The image products of modern space-borne SAR instruments used for earth observation have to support the diverse requirements of the multi-discipline SAR user community. In general, some users prefer radiometrically enhanced lower resolution images (corresponding to a high number of looks), while other applications primarily call for high spatial resolution (where we think of a lower number of looks) [1], [2]. This is why many SAR projects often offer a range of products in parallel; however, in our case we are mainly interested in efficient feature extraction and comparative classification rather than in the availability of numerous products tailored to a variety of other applications.

The classification of high resolution SAR images is a demanding task especially for 1 m resolution data, as many window-based texture processing algorithms fail in the presence of high resolution scattering details and partly developed speckle noise. In particular, urban scenes of densely built-up areas pose a number of challenges that may call for classification using reduced resolution image data. A reason for using reduced resolution data could be to average out small annoying details preventing us from seeing typical texture patterns extending over larger scales.

Thus, we begin with a short overview of SAR specific feature extraction and classification and the requirements of our applications. In contrast to these expectations, we summarize what kind of products a typical modern SAR mission offers as

products. Then we demonstrate what type of product we need and how it can be generated – either in the complex or in the intensity domain. Adapting the number of looks without the generation of detrimental artifacts seems to be the best way to accomplish our goals. This approach will be verified by analyzing a number of TerraSAR-X images [3].

II. FEATURE EXTRACTION FROM SAR IMAGES

When SAR high resolution images are to be used for feature extraction and subsequent unsupervised surface cover classification, we need in particular:

- High geometrical resolution and fidelity (i.e. no degraded edges) with negligible layover effects
- High radiometric data quality with low speckle and thermal noise (i.e. good signal-to-noise ratios), without aliasing or Gibbs artifacts incurred during product generation
- Data without corner reflector and calibration effects.

However, from a product viewpoint, the needs listed above may represent conflicting requirements. Radiometrical and geometrical quality often preclude each other in conventional products. In addition, most users don't question about calibration quality and re-sampling effects; however, classification relies on comparable (i.e. calibrated) and radiometrically reliable data.

Several well-known publications have shown that the specific properties of SAR data have to be taken into account before we can start with SAR image data analysis: one needs a successful identification and localization of lines and edges; texture extraction and scene segmentation have to cope with high radiometric contrast levels and speckle phenomena. For instance, a classical approach for edge detection in SAR images is described in [4], a watershed approach to support image segmentation in [5], and speckle reduction by Gamma and Gaussian MAP filtering approaches can be found in [6] since for many image classification tasks, uncorrected speckle noise contained in SAR images prevents a robust determination of land cover or urban scene characteristics. On the other hand, these well-known algorithms hinge on the assumed basic speckle distribution such as a Gamma law.

Alternative approaches of wavelet-based and enhanced model-based despeckling (EMBD) are described and applied in [7], [8], and [9].

In general, users assume that the available data show uncorrelated (i.e. un-smearred) speckle. This, however, is not the case when we have a more detailed look at typical SAR images. When we want to make full use of the available data, for instance, when we apply EMBD filtering, we have to provide uncorrelated speckle. This necessitates the generation of new products with high radiometric and geometric quality. The necessary number of looks and the attainable quality can be estimated by a Cramer-Rao approach [10].

III. SHORT OVERVIEW OF TERRASAR-X PRODUCTS

When we compare the requirements given above with the available range of products offered by the German TerraSAR-X mission, we see immediately that the pixel resolution and the effective number of looks of the products vary considerably.

The basic TerraSAR-X imaging modes are:

- Stripmap mode (“SM”) in single or dual polarization
- ScanSAR mode (“SC”) in single polarization
- Spotlight mode (“SL”) in single or dual polarization
- High Resolution Spotlight mode (“HS”) in single or dual polarization.

TABLE I
BASIC TERRASAR-X IMAGING MODE PARAMETERS

Imaging Mode	Incidence Angle (full performance) [deg.]	Azimuth Resolution [m]	Ground Range Resolution [m]	Effective Number of Looks (see text)
SM	20 - 45			
Single Polarization		3.5 - 3.3	3.5 - 3.3	1.0 - 1.3
Dual Polarization		6.6 - 6.6	6.6 - 6.6	1.8 - 2.8
SC	20 - 45	19.2 - 18.5	19.2-17.0	5.6 - 11.1
SL	20 - 55			
Single Polarization		3.5 - 1.7	3.5 - 1.7	2.0 - 1.2
Dual Polarization		3.5 - 3.4	3.5 - 3.4	1.0 - 2.4
HS	20 - 55			
Single Polarization		1.8 - 1.1 (at 300 MHz)	1.8 - 1.1 (at 300 MHz)	1.5 - 1.2 (at 300 MHz)
Dual Polarization		3.3 - 2.2	3.3 - 2.2	1.5 - 1.5

The TerraSAR-X products of the basic imaging modes can

be ordered as detected data or as single look complex data. Detected data are offered either in ground range projection, or in geocoded map geometry with ellipsoidal corrections, or geometrically map and terrain corrected using a digital elevation model, while the single look complex data are available in slant range geometry only. In addition, all detected data (except for the radiometrically enhanced SC products) can be obtained either as spatially enhanced or radiometrically enhanced products.

Table I shows the basic parameters of the TerraSAR-X imaging modes. (All numbers are taken from [3]). Within the azimuth and ground range resolution ranges, the first resolution corresponds to the smallest given incidence angle, while the second one refers to the largest given incidence angle.

The effective numbers of looks are defined for detected data of a spatially enhanced product within the given range of incidence angles. (Radiometrically enhanced products would have a much higher number of looks). In addition, Table II shows the radiometric resolution of every imaging mode.

Our primary interest aimed at image data with high resolution and low speckle. This led to our first choice of spatially enhanced Single Polarization High Resolution Spotlight (“HS”) mode data. They offer best geometrical resolution within a wide range of incidence angles, together with good radiometric resolution and an acceptable effective number of looks. We selected both single look complex as well as detected geocoded ellipsoid corrected data. In the latter case, these data permit direct spatial comparisons on a common sampling grid despite the fact that all data have to undergo a geometrical re-sampling procedure.

TABLE II
RADIOMETRIC RESOLUTION OF THE IMAGING MODES

Imaging Mode	Incidence Angle (full performance) [deg.]	Radiometric Resolution [dB]
SM	20 - 45	
Single Polarization		3.1 - 2.9
Dual Polarization		2.5 - 2.1
SC	20 - 45	1.6 - 1.2
SL	20 - 55	
Single Polarization		2.4 - 3.1
Dual Polarization		3.1 - 2.4
HS	20 - 55	
Single Polarization		2.7 - 3.1 (at 300 MHz)
Dual Polarization		2.7 - 2.8

On the other hand, we must be aware that the basic HS products do not yet provide us with sufficiently reliable data for feature extraction and unsupervised surface cover classification. To this end, we have to generate a high quality product based on uncorrelated speckle.

IV. CREATING A NEW PRODUCT

The challenge is to combine in an automated procedure low speckle with high resolution aiming at a new SAR image product to be derived from the existing product data. Signal processing theory can help us to reach this goal: We can sacrifice spatial resolution as long as we need better radiometrical quality. In essence, this results in a classical multilooking approach; however, we have to be very careful to avoid any potential aliasing and Gibbs phenomena arising during our product generation.

If we proceed in a two-step controlled fashion as described below, the given approach serves as a recipe how to proceed.

A. Bandwidth Adaptation and Uncorrelated Speckle

During a first step, the available bandwidth of an image is fully exploited to remove redundant information. Based on image metadata, we verify and adapt the image resolution and the pixel spacing in both directions of the image (small discrepancies between range and azimuth resolution may remain unaccounted for). As a result of this first step, we may end up with images of reduced size.

The bandwidth adaptation may be performed using complex-valued or detected data. If we use complex-valued data and apply Fourier transform methods we must assure sufficient zero padding to obtain correct results. If we use detected data, we must care for low-pass filtering prior to any down-sampling.

Next, we need uncorrelated speckle (i.e. no speckle smearing across pixels). Speckle correlation may have been induced, for instance, by re-sampling of a detected image during geometric image projection on a regular grid. The generation of uncorrelated speckle can be accomplished by simple sub-sampling of an image (e.g., by leaving out every second line and column). The effectiveness of this speckle decorrelation step has to be verified by pixel autocorrelation analysis in homogeneous areas.

Now one can now perform image despeckling by a state-of-the-art algorithm (e.g., an EMDB technique [8]). We have to note, however, that the speckle correlation may vary from near to far range of a SAR image. Therefore, in our present studies we concentrated on a limited range of comparable incidence angles where we can assume a near constant speckle correlation. During further analysis, we will extend our work to spatially variant speckle correlation.

B. Sub-Sampling Tailored to Classification Algorithms

If we want to classify targets into object classes, best classification results will be obtained when the scale of the targets is adapted to the classification algorithm.

In many cases, high SAR image resolution does not result in good classification results; classification algorithms based on textures should see the full texture features on all scales being exploited by the algorithms. Excessively high resolution may lead to irregular fine scale details that mask existing textures. Hence, another image sub-sampling step may be required depending on the needs of our classification algorithms.

Again, a new sub-sampling has to follow the classical rules of information theory. A Gibbs-free data reduction can be obtained by careful selection of spectral cut-off techniques after low pass filtering. One can verify this step by checking the equivalent number of looks of the output images and the preservation of edges. Table III shows typical results after filtering and sub-sampling of complex-valued TerraSAR-X images.

C. Complex vs. Detected Data

In principle, one can use complex-valued data or detected data for steps A and B, however, complex-valued data are our “silver bullet” as they allow the perfectly controlled generation of all intermediate products within a processing chain. Detected data are our second choice. In this case, we have to rely on data with (possibly unknown) pre-processing and aliasing effects.

V. EVALUATION BY TYPICAL EXAMPLES

Fig. 1 depicts a TerraSAR-X urban sub-scene of Gizeh in Egypt close to the Pyramids (radiometrically scaled data, no despeckling) containing a variety of mostly diagonal image structures.

Fig. 2 demonstrates that we have higher correlation (i.e. denser sampling) in the range direction (data derived from complex original product data of Fig. 1).

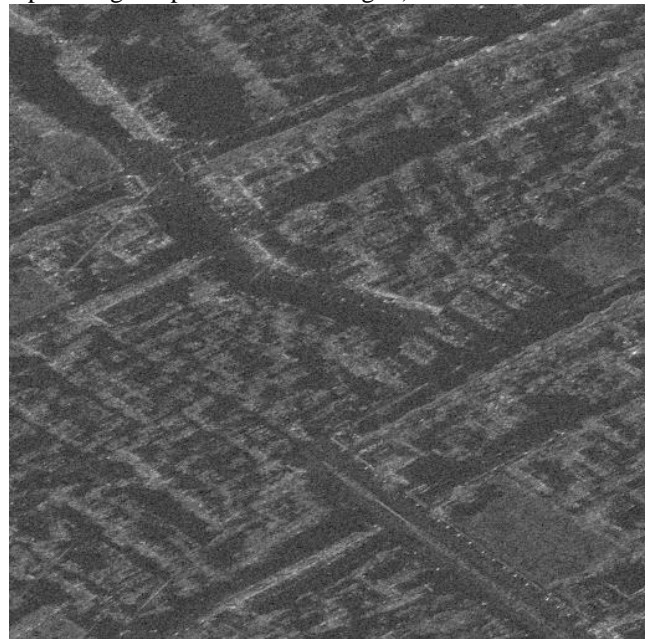


Fig. 1. A TerraSAR-X sub-scene of Gizeh, Egypt.

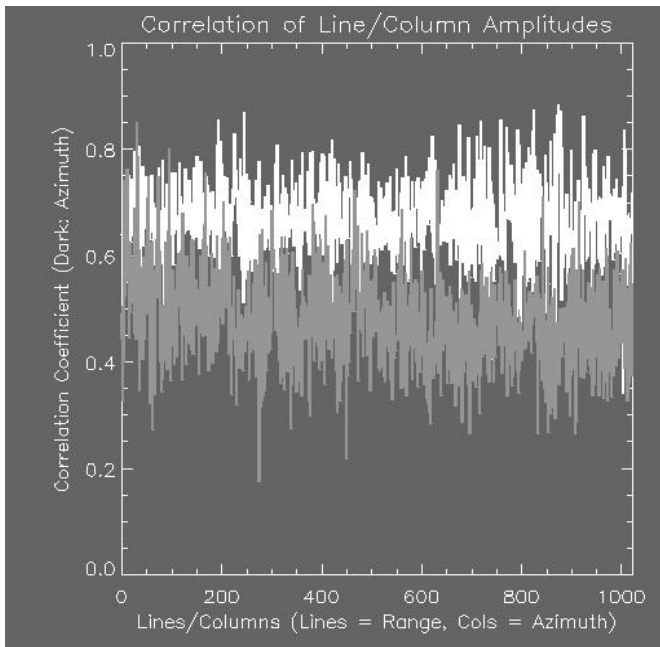


Fig. 2. Correlation along range and azimuth.

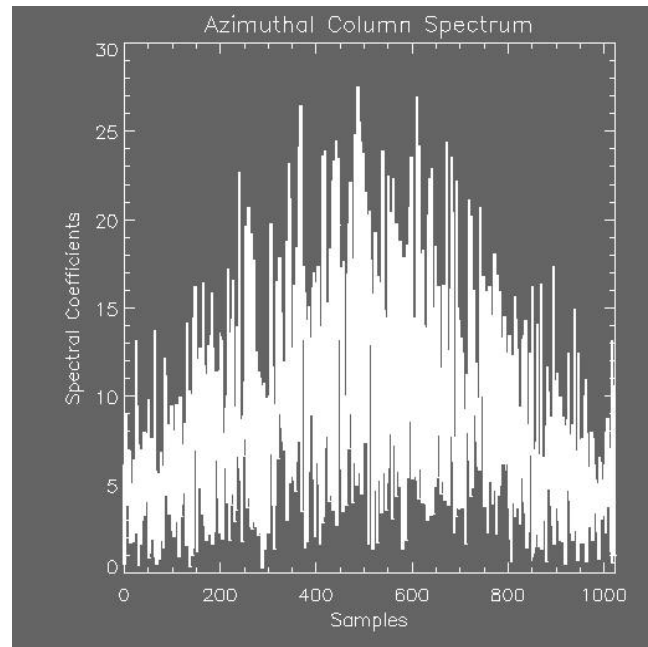


Fig. 4. Typical Fourier spectrum of an image column along azimuth.

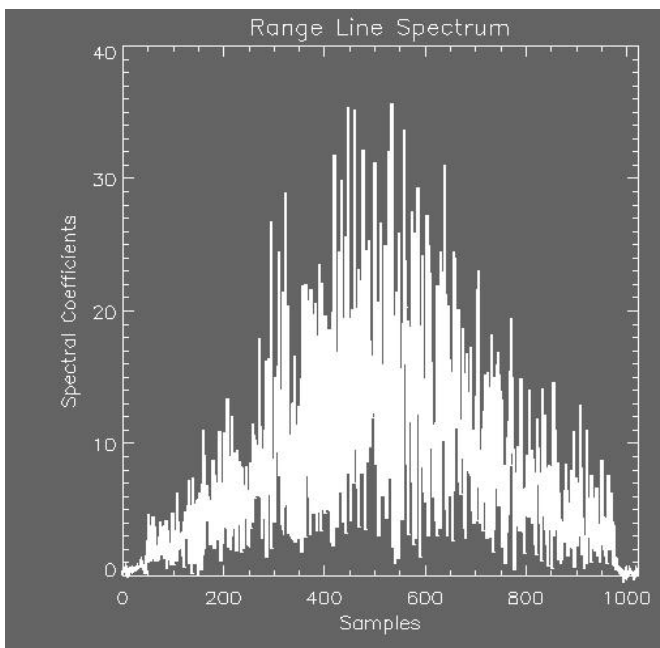


Fig. 3. Typical Fourier spectrum of an image line along range.

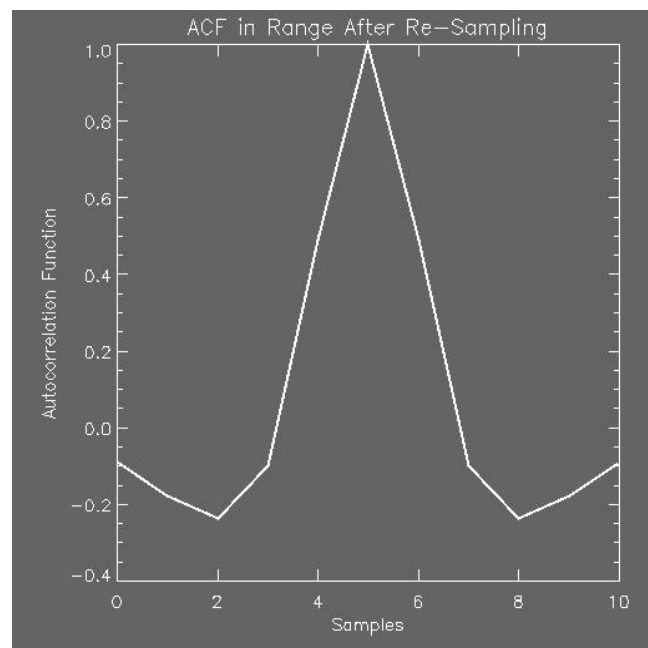


Fig. 5. Typical sample autocorrelation function along range.

Figs. 3 and 4 illustrate that we can profit from the different spectral characteristics in range and azimuth direction: we can clip bandwidth in range direction (see the spectral falloff near the first and the last samples of Fig. 3). When done properly, this should not compromise image quality.

Fig. 5 shows that after proper sub-sampling as described above the autocorrelation characteristics become rather uniform. What we get are reliable input data for un-supervised image classification.

Of course, the sub-sampling leads to an increase of the equivalent number of looks. Table III summarizes typical results of different surface cover types to found in the vicinity of the sub-scene shown in Fig. 1. There one can find extended nearly homogeneous areas containing bright and dark sandy areas and even some radar shadow behind a pyramid. We assume that these areas are nearly flat without pronounced topographic effects. The steady increase in the number of looks is indicative of regular conditions.

TABLE III
EQUIVALENT NUMBER OF LOOKS AFTER SUB-SAMPLING

Image Resolution	No. of Looks: Bright Sand Target	No. of Looks: Dark Sand Target	No. of Looks: Radar Shadow Zone
Original Res. 1.2 m	0.98	0.98	0.86
Reduced Res. 2.6 m	4.29	4.81	3.86
Reduced Res. 4.0 m	10.68	11.77	8.40

VI. ANALYSIS OF TEXTURE PARAMETERS

Once the basic processing steps described in Section IV have been done, we can verify the usefulness of our approach for texture analysis. As a typical example, we again concentrate on another sub-scene of our Gizeh image that contains a lot of settlement structures.

The selected sub-sampled area can be seen in Fig. 6a, the same area after despeckling is shown in Fig. 6b. (The usefulness of despeckling is also shown in a companion paper [9]).



Fig. 6:
a) Top: Test scene after sub-sampling,
b) Bottom: Test scene after additional despeckling.

This is our basis from which to start with texture analysis. What can be verified first are the directional texture parameters derived from selected scenes.

To this end, EMBD filtering with various analyzing window sizes and model orders have been conducted. These tests verified that our concept described in Section IV permits a reliable texture classification. As expected, it turned out that the selected window size determines the granularity of our solution, while the model order determines the complexity of details to be fitted.

A window size of 21×21 pixels and a model order of 3 seem to be a good compromise allowing for fast processing and compact classification.

In the example shown in Fig. 7, a window size of 21×21 pixels and a model of order 2 were used. Fig. 7a and Fig. 7b illustrate the complementary appearance of the resulting vertical and horizontal texture parameters. In addition, Figs. 8a and 8b contain the diagonal texture parameters. Again, the parameters of the upper and lower diagonal directions complement each other. This can serve as an additional verification step of the EMBD results.

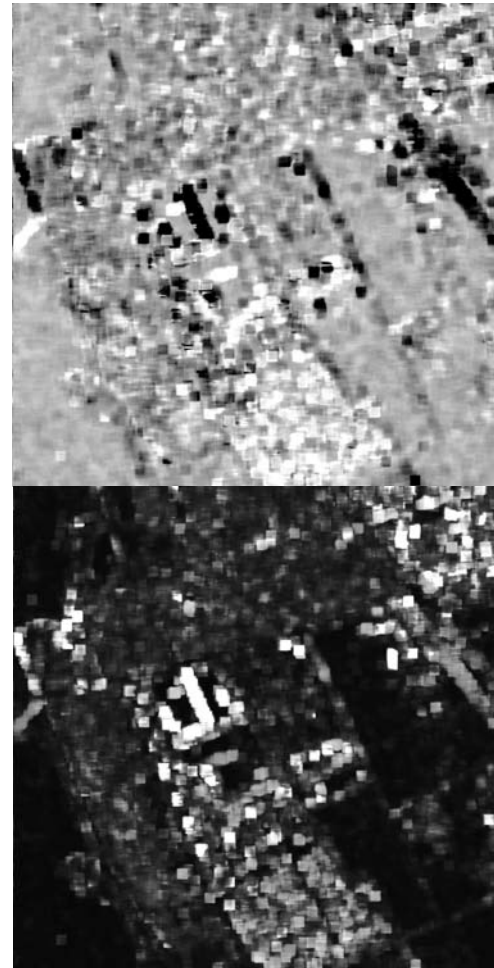


Fig. 7:
a) Top: Vertical texture parameters,
b) Bottom: Horizontal texture parameters.

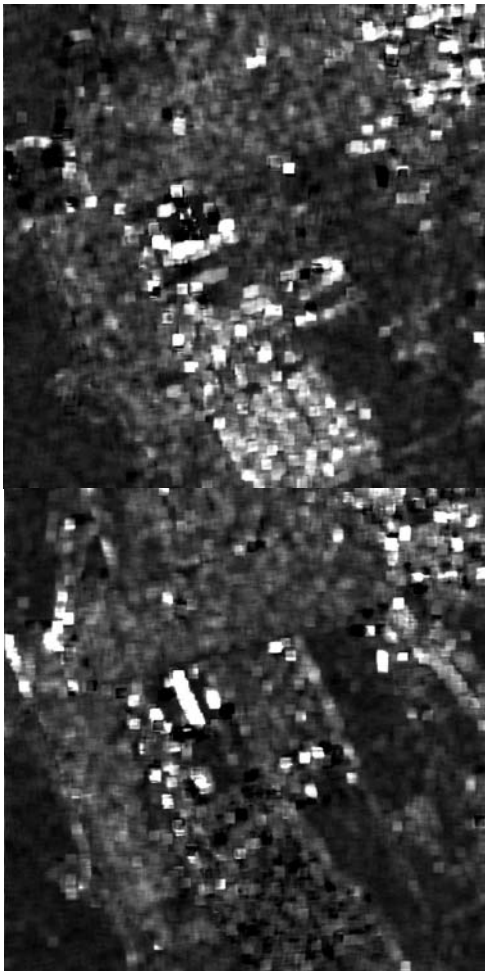


Fig. 8:
 a) Top: Upper diagonal texture parameters,
 b) Bottom: Lower diagonal texture parameters.

VII. OUTLOOK

More tests with diverse scene contents are prime candidates for the general validation of our proposed concept. In particular, the interpretation of changes contained in image time series and the identification of moving objects are becoming more and more attractive in image processing. The inclusion of these topics in texture analysis of SAR data represents an interesting long term goal.

VIII. SUMMARY

The quality of the proposed new product depends on the information-theoretical correctness of the applied sub-sampling methods. Single-look complex data offer the perspective of sufficient zero padding in the Fourier domain during processing. Therefore, a product generation based on complex data appears most promising.

ACKNOWLEDGMENT

The TerraSAR-X images have been provided by DLR under an approved TerraSAR-X research proposal [11].

REFERENCES

- [1] M. Skolnik, *Introduction to Radar Systems*, Third Edition, New York: McGraw-Hill, 2002.
- [2] C. J. Oliver and S. Quegan, *Understanding Synthetic Aperture Radar Images*, Raleigh NC: Scitech, 2004
- [3] http://www.dlr.de/tsx/documentation/SAR_Basic_Products.pdf
- [4] R. Touzi, A. Lopes, P. Bousquet, "A statistical and geometrical edge detector for SAR images", *IEEE Trans. Geoscience and Remote Sensing*, vol. 26, pp. 764-773, Nov. 1988.
- [5] L. Vincent, P. Soille, "Watersheds in digital spaces: An efficient algorithms based on immersion simulations", *IEEE Trans. Pattern Analysis and Machine Intelligence*, vol. 13, pp. 583-598, Jun. 1991.
- [6] Sarmap, *The SAR-Guidebook*, Oct. 2007, http://ittvis.com/envi/pdfs/SAR_Guidebook.pdf
- [7] A. Achim, P. Tsakalides, A. Bezenarianos, "SAR Image Denoising via Bayesian Wavelet Shrinkage based on Heavy-Tailed Modeling", *IEEE Trans. Geoscience and Remote Sensing*, vol. 41, pp. 1773-1784, Aug. 2003.
- [8] M. Quartulli, M. Datcu, "On the quality of model based information extraction from SAR images", *Proc. SPIE*, vol. 4543, pp. 94-99, 2002
- [9] G. Schwarz, Daniela Molina Espinoza, M. Datcu, "A new look at feature selection", *these proceedings*, 2008.
- [10] http://en.wikipedia.org/wiki/Cramer_rao_bound
- [11] http://sss.terrasar-x.dlr.de/how_to_submit_a_tsx_proposal.pdf.